nature geoscience

ARTICLES

https://doi.org/10.1038/s41561-018-0066-z

Puzzling features of western Mediterranean tectonics explained by slab dragging

Wim Spakman[1,2*], Maria V. Chertova[1], Arie. van den Berg[1] and Douwe J. J. van Hinsbergen[1]

The recent tectonic evolution of the western Mediterranean region is enigmatic. The causes for the closure of the Moroccan marine gateway prior to the Messinian salinity crisis, for the ongoing shortening of the Moroccan Rif and for the origin of the seismogenic Trans-Alboran shear zone and eastern Betics extension are unclear. These puzzling tectonic features cannot be fully explained by subduction of the east-dipping Gibraltar slab in the context of the regional relative plate motion frame. Here we use a combination of geological and geodetic data, as well as three-dimensional numerical modelling of subduction, to show that these unusual tectonic features could be the consequence of slab dragging—the north to north-eastward dragging of the Gibraltar slab by the absolute motion of the African Plate. Comparison of our model results to patterns of deformation in the western Mediterranean constrained by geological and geodetic data confirm that slab dragging provides a plausible mechanism for the observed deformation. Our results imply that the impact of absolute plate motion on subduction is identifiable from crustal observations. Identifying such signatures elsewhere may improve the mantle reference frame and provide insights on subduction evolution and associated crustal deformation.

Crustal deformation induced by plate subduction is typically considered in the context of the relative motions between two converging plates: both trench-perpendicular plate motions, such as slab rollback or slab advance, and trench-parallel movements cause the crust to deform[1–3]. However, the absolute motions of plates place additional lateral forces on the subducting slab. Absolute plate motions (APMs) at the surface can act to push or pull the subducting slab in the mantle in directions different to that of the relative plate convergence. This slab dragging[4] is resisted by the mantle and the resistance can translate into further crustal deformation at the surface. Generally, slab dragging denotes the process of lateral slab transport through the mantle that is forced by the absolute surface motion of the subducting plate. A simple analogy of slab dragging would be a hand (the slab) dragging through water (the mantle) by the motion of one's arm (the surface motion of the subducting plate). The mantle resistance to slab dragging comprises the resistance to trench-parallel slab motion through the mantle and also incorporates slab anchoring[1], which classically concerns only the mantle resistance to trench-perpendicular slab motion.

Remarkably, since the recognition of plate tectonics only a few suggestions of slab dragging have been made. These studies[5–8] imply that on timescales of tens of millions of years, slab dragging can potentially laterally transport entire subduction systems hundreds of kilometres in a direction that is governed by the absolute surface motion of the subducting plate and not by the relative plate convergence. Mantle resistance against slab dragging may strongly affect subduction evolution and lithosphere deformation[4–8], but remains underexplored. Here we argue that enigmatic tectonic features in the western Mediterranean that were activated predominantly in the past ~8 Myr, and some of which continue to deform today, can be explained by slab dragging.

Puzzling tectonic features of the western Mediterranean region

The dynamic role of subduction in the tectonic evolution of the western Mediterranean region has been long debated[9]. Considerable focus was obtained with the delineation of the Rif–Gibraltar–Betics (RGB) slab by seismic tomography[10–14] (Fig. 1 and Supplementary Video 1). This provided a clear target for tectonic reconstruction[15–17] and three-dimensional (3D) slab-evolution modelling[14], which demonstrated that a westward subduction rollback was a prime driver of tectonic evolution in the Neogene. The slab settled in the Betic–Alboran–Rif region in the Late Miocene (~8 million years ago (Ma)) with no geological evidence for further lateral motion[14,16,17], whereas slab sinking was accompanied by progressive slab tearing from the eastern to the central Betics[11,18,19] and by progressive delamination of the lithospheric mantle[18,20]. From the western Betics to the Moroccan Rif, the intermediate-depth seismicity (Fig. 2a) testifies to a still-attached slab[18,21].

The specific role of the slab in determining regional tectonics is, however, still equivocal. In fact, most tectonic activity since the Late Miocene is attributed to the relative NW–SE convergence between the African and Iberian (Eurasian) plates along an undefined plate boundary geometry[22–24]. Although this may explain some general features, such as regional rotations in the stress field, regional trends in global positioning system (GPS) motions or the sense of motion on important fault systems[23,25,26], there is no integral explanation for the important first-order tectonic features that characterize the RGB region.

These puzzling features comprise the closure of the marine gateways in northern Morocco prior to the Messinian salinity crisis[27] (MSC) by an on average N–S crustal shortening[28], the enigmatic present-day NNE–SSW shortening shown by GPS motions[24,29] and crustal thickening of the Moroccan Rif[24,30–32], the geodynamic origin of the regionally most prominent faults systems (the seismically active west Trans Alboran Shear Zone (WTASZ)[33] and the Eastern Betics Shear Zone (EBSZ), the WSW–ENE extension of the central–eastern Betics[18,34] and, lastly, the contrasting main tectonic shortening directions of the Rif and Betic orogens[9] (Fig. 2b).

Solutions for the neotectonic role of the slab in explaining some of these features have been suggested from numerical modelling of the

[1]Department of Earth Sciences, Utrecht University, Utrecht, The Netherlands. [2]Centre of Earth Evolution and Dynamics (CEED), University of Oslo, Oslo, Norway. *e-mail: w.spakman@uu.nl

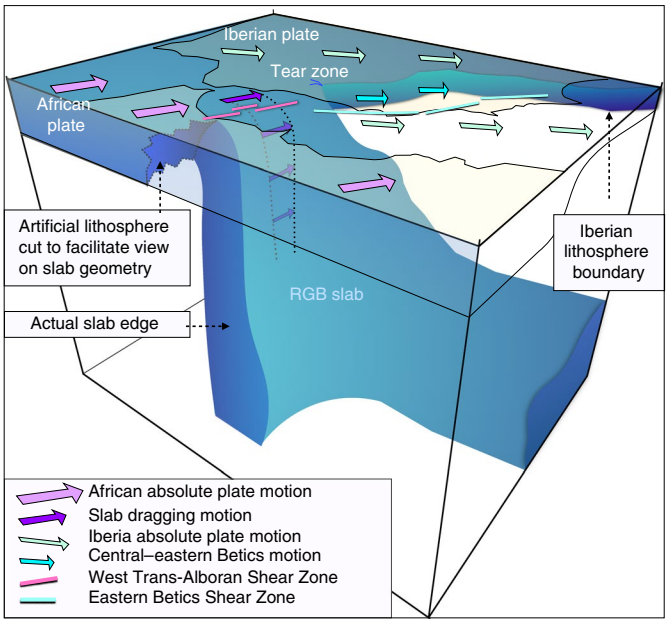

Fig. 1 | RGB slab and its connectivity to the African and Iberian lithosphere. Cartoon interpretation of the RGB-slab morphology[10–14,18] across the upper mantle. Vectors illustrate the APMs for Africa and Iberia[37] as well as the slower central–eastern Betics motion. A N–NNE slab dragging motion by the absolute motion of predominantly the African plate, is suggested in the slab. The bottom is at a depth of 660 km.

lithosphere that treats the lithosphere as a thin elastic[24] or viscoplastic[23,35] sheet using the relative NW–SE plate convergence as a boundary condition. The elastic modelling requires an approximately SSW directed traction positioned locally under the Moroccan Rif to explain the anomalous GPS motions of the Moroccan Rif, which is attributed to an approximately SSW rollback of the delaminated African continental lithosphere[24]. The viscoplastic modelling of the wider plate boundary region suggests either no role for the slab[35] or requires an approximately SW-directed shear traction under the Alboran domain, which is attributed to slab suction and/or slab-induced mantle flow[23]. Furthermore, a W–WSW-directed slab rollback is suggested to explain the kinematics of the subduction wedge to the west of the Gibraltar Strait[22]. These and other studies exemplify that the proposed dynamic role of the RGB slab is quite diverse and that it is invariably being cast in a regional relative plate motion frame. However, slab motion and mantle flow can only be properly defined and investigated in the mantle reference frame[1,2], which is the framework we use here for our investigation of the dynamic role of the RGB slab in driving the regional tectonic evolution. To this end, we compare predictions of slab motion from 3D numerical models of RGB subduction evolution with the first-order observations of regional tectonic change in the western Mediterranean in the past ~8 Myr, including the noted puzzling tectonic features.

4D modelling of mantle-resisted RGB slab dragging

Our numerical subduction models incorporate published models[4,14] as well as new models that together test the model sensitivity for a wide range of rheological settings, initial conditions and APM constraints[4,14] (Methods). The mantle frame and associated APM plays an important role in our modelling, but is still rather uncertain. Figure 3 illustrates this uncertainty with the APM predictions of eight modern mantle frames for a point that is assumed to be located on the African plate. Models based on the hotspot–plume paradigm[36–39] generally show N–NNE African plate motion, of which models restricted to Indo-Atlantic hotspots[36,38] predict APMs with a slightly larger azimuth and amplitude. The other APM models, which predict that APM vectors point to the NW–NNW, are based on alignment with fast directions of upper mantle anisotropy[40–42], or alignment with ocean spreading directions[42]. We prefer hotspot mantle frames because, by their nature, these anchor APMs to the deep mantle. We emphasize that all mantle frames predict a northern component of the African APM in the region. Here, we used for most of our modelling the global moving hotspot reference frame (GMHRF)[37] mantle frame for the African APM, but we have also experimented with mantle frames in which Africa is fixed to the mantle or moving to the NW[4]. The Iberian APM is schematically shown in Fig. 1 and is constrained by adding its NW–SE-directed relative motion vector obtained from plate reconstruction[16] (for numerical modelling) or from GPS motions[34,43] (for our GPS analysis) to the African APM.

The primary modelling results are that a rheologically strong slab is required to optimize the match between the predicted and observed slab geometry and that the RGB slab must still be attached to both the African and the Eurasian plates[14] (Fig. 1 and Supplementary Videos 3 and 4). The latter concurs with seismological and geodetic observations[18,34] and with the fragmented plate boundary of widely distributed active faults. The connectivity between the slab and the plates causes the component of the APM that is shared by the two plates to transport the entire region northward, which may include a comparable transport of the slab laterally through the mantle (Fig. 1). Such slab dragging is, indeed, what our numerical experiments of slab evolution invariably reveal (Fig. 4, Supplementary Fig. 1 and Supplementary Videos 2–4), which concurs with previous models using different model set-ups and mantle rheology[4,14]. In the GMHRF frame, the modelled slab dragging occurs to the N–NNE from ~8 Ma and is undetectable from the relative NW–SE plate convergence (Fig. 4a, inset). In the models, the slab dragging results predominantly from the push by the African lithosphere because the Iberian lithosphere, although moving to the NE, is also converging towards Africa in the SE direction. The effect on the N–NNE slab dragging is, however, reduced by continuous lithosphere tearing that has gradually developed under the eastern Betics and propagates to the west (Fig. 4a and Supplementary Video 2).

The various subduction models determined here (Methods) and previously[4,14] all share the first-order feature of RGB slab dragging by the African APM. Earlier models[4], testing different APM frames, show that if the Africa motion was to the NW (Fig. 3), the slab is dragged accordingly to the NW, and if Africa is fixed to the mantle no slab dragging occurs. This substantiates that the APM of the subducting plate governs the direction of the RGB slab dragging. Importantly, our models show that the viscous coupling with the mantle resists slab dragging, which causes the slab to lag slightly behind with the APM of the African plate leading to an indentation of the Moroccan margin by the slab (Fig. 4a). This is corroborated by models with a slightly higher mantle viscosity that feature the slab indentation of the African margin to a larger degree, as shown by the B model of Supplementary Fig. 1 and in previous work[4,14]. We conclude that mantle-resisted slab dragging is a robust model feature that is used in the following as a novel guidance for investigating the causal links with regional tectonic change evidenced by the regional deformation of the crust coupled to the slab and coupled to the African and Iberian lithospheric mantle.

Matching predictions of slab dragging to tectonic change

Tectonic reconstruction shows that during the rapid phase of overall westward rollback prior to ~8 Ma, the Alboran platelet that is coupled to the slab moved between and thrusted over both the African and Iberian margins[9,16]. When the modelled slab evolution is viewed relative to the African plate, which is important for linking model predictions to the tectonics of the African margin, the slab moves

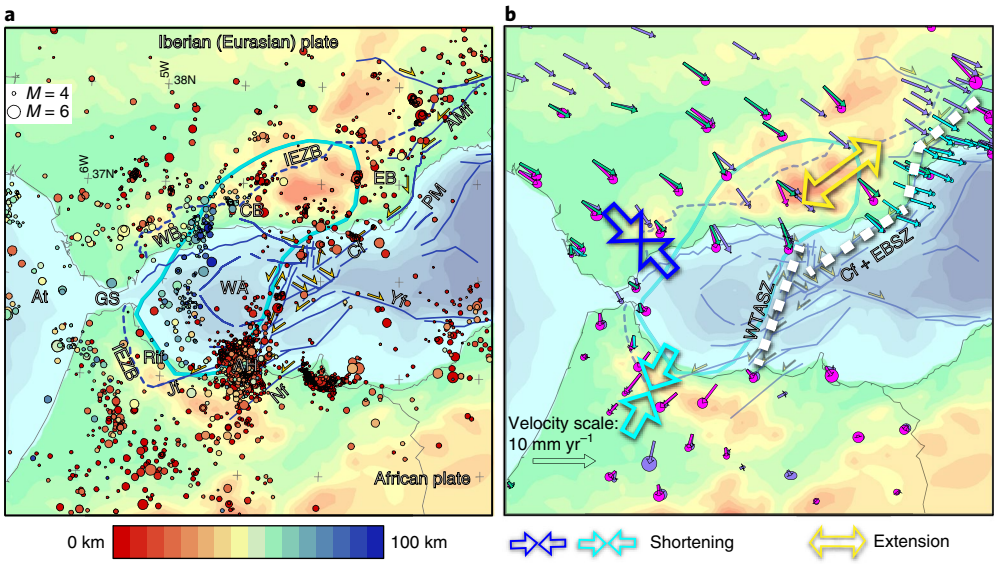

Fig. 2 | Western Mediterranean plate boundary region. a, Seismicity (http://www.ign.es/web/ign/portal) with magnitude $M > 3$ and with the hypocentre depth colour coded (legend). Light blue line: slab outline at 200 km (ref. [14]); dashed blue lines: internal–external Betics zone boundary (IEZB)[9]; dark blue lines: major strike-slip faults[18] with the sense of motion indicated by yellow half arrows. **b**, Major styles of tectonic deformation from ~8 Ma and GPS motion vectors in an African-fixed frame: purple[34], green[48], light blue[47], magenta[43]. AH, Al Hoceima earthquake cluster; AMf, Alhamade–Murcia fault; At, Atlantic Ocean; CB, Central Betics; Cf, Carboneras fault system; EB, Eastern Betics; GS, Gibraltar Strait; Jf, Jehba fault; Nf, Nekor fault; PM, Palomares margin; Rif, Moroccan Rif; WA, West Alboran; WB, Western Betics; Yf, Yusuf fault.

initially to the SW when westward rollback is still important, and in the past 8 Myr to the S–SSW (Fig. 4b). The relative S–SSW convergence between the modelled RGB slab and the African plate is due to the viscous mantle resistance against the N–NNE slab dragging, which causes the slab to lag behind (Fig. 4a).

Prior to ~8 Ma, westward rollback in the African frame combines with this S–SSW-directed component of slab motion (Fig. 4b) and predicts the effective approximately SW strike and left-lateral motion of the Jehba and Nekor faults that bound the Alboran platelet to the SE, as well as the ENE–WSW thin-skinned thrusting that accommodates a large shortening in the Rif at the Alboran–Africa plate interface[9,44]. Slab-edge indentation along the African margin due to mantle-resisted slab dragging also provides the forcing mechanism for the proposed delamination and destruction of the African continental edge during a rapid westward rollback[20,45] (Supplementary Videos 3 and 4). In an Iberian-fixed frame, the slab seemingly moves initially westward under the Betics and then to the NW (Fig. 4c). In this frame the relative plate convergence combines with a seemingly NW-directed slab dragging. Geological observations show an overall WNW shortening direction[9,44] turning to NW from ~8 Ma when rollback stalled (Fig. 4c). These relative slab–plate motions (Fig. 4b,c) provide, in combination with relative plate convergence, a dynamic driver for the disparate directions of the mean tectonic transport in the Betic and Rif[9,44].

After ~8 Myr, the rollback rates sharply decreased and the slab indentation of the north Moroccan margin became the dominant driver of deformation, which provides a straightforward explanation for the puzzling local crustal thickening of the Rif at the continuation of the slab with the continent[30–32]. The roughly N–S-directed, kilometre-scale, thick-skinned thrusting of the Rif from ~8 Ma (ref. [28]) complies entirely with the direction and modelled magnitude of indentation of the slab edge into African continental lithosphere. Thrusting occurred along steep reverse faults[28] and incited a large uplift for which a shortening of 10–20 km is thought sufficient to close the Moroccan marine gateways that precede the MSC[27,28]. The 10–15 km of indention modelled in our G model (Fig. 4a) can thus provide the missing dynamic mechanism that forces the Moroccan gateway closure.

Mantle-resisted slab dragging also explains the existence of the left-lateral TASZ. The WTASZ, striking N 22.5° E±2.5°, is presently the seismically most-active part[33] and lines up with the eastern boundary of the imaged slab (Figs. 2 and 3). The NE–SW strike of TASZ faults directly to the east of the WTASZ (Figs. 2 and 3) complies with the earlier rapid rollback phase (see the Jehba and Nekor faults). The WTASZ accommodates the differential motion between, on one side, the west Alboran and western Betics crust

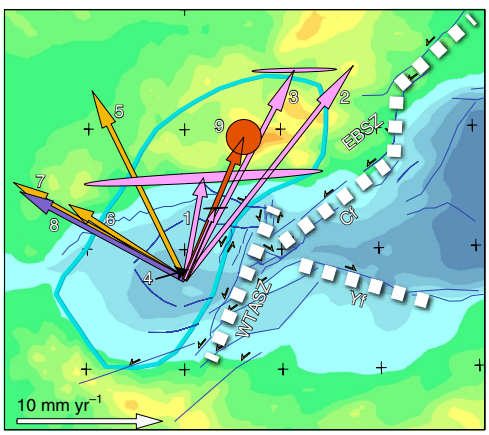

Fig. 3 | African APM estimates from modern APM models. Hotspot-based models: 1, GMHRF[37]; 2, Indo-Atlantic Moving Hotspot Frame[36]; 3, Indo-Atlantic hotspot frame[38]; 4, HS4-EW-MOVEL56 global fixed-hotspot frame[39]. Alignment with mantle anisotropy: 5, SL2013SVA[42]; 6, SKS-MORVEL[41]; 7, DR2012[40]; 8, SARF ocean-spreading alignment[42]; 9, APM of the African plate determined here. 1-σ confidence ellipses are plotted when available. Thick dashed transparent lines show the key fault system (the caption to Fig. 2 describes the lines). Vectors are computed for (3.5° W, 36° N), but are displayed at (4.0° W, 35.75° N).

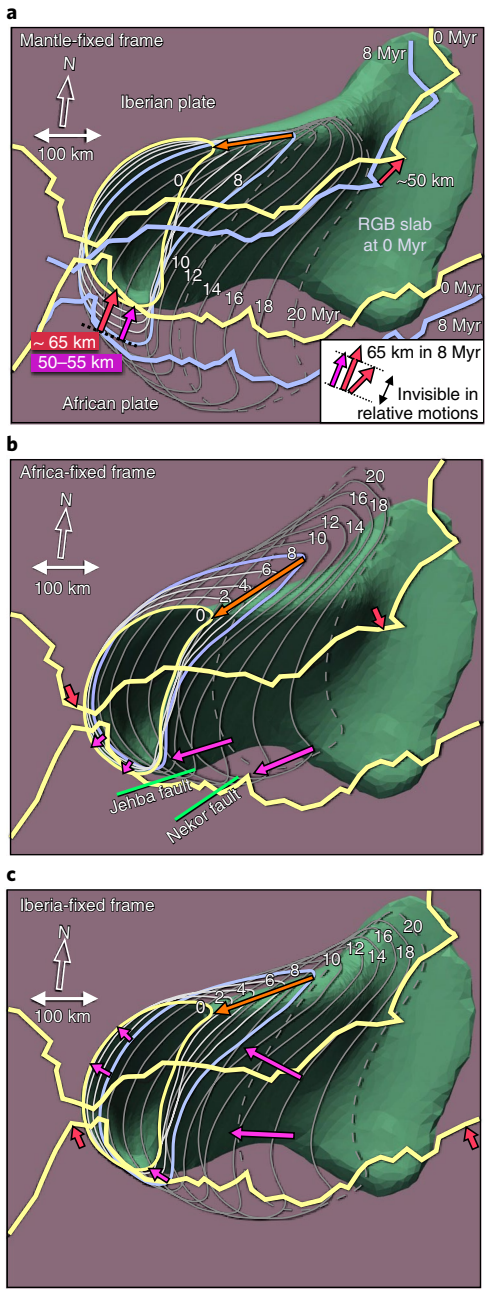

Fig. 4 | G model: slab motion with a focus on the past 8 Myr. a, Slab motion in a mantle reference frame. The 1,400 K slab envelope is shown from 200 km downward. Grey contours at every 2 Myr since 20 Ma track the slab motion. Purple and yellow lines: slab and plate positions at 8 and 0 Myr, respectively; magenta vector: slab transport by mantle-resisted slab dragging; inset: comparison of movement vectors. **b**, Slab motion in the Africa-fixed frame. Magenta vectors: WSW convergence until ~8 Myr followed by a SSW–S directed slab indentation. **c**, Slab motion in the Iberia-fixed frame. Magenta vectors: W–NW-directed slab motion through time. In all of the panels, the vectors show motions in ~8 Myr—red: movement of Iberia and Africa; orange: slab tearing ~120 km in **a**, and ~150 km in **b** and **c**.

coupled to the still-continuous slab and, on the other side, the east Alboran crust that can move more freely relative to the slab with Africa and Iberia (Eurasia).

Lastly, the central-to-eastern Betics extension is explained by the relative motion between the NE-directed absolute motion of the Iberian main continent (Fig. 1) and the slab that lags behind because of mantle resistance against the NNE transport and is decoupled from Iberian motion by continuous slab tearing (Fig. 4a,c). West of the slab tear, at ~4° W, the crust is still locked to the slab[18] and the Iberian lithosphere and NW–SE shortening from the relative plate convergence dominates. In contrast, the central–eastern Betics crust to the east lacks the support of the lithospheric mantle[18] (Fig. 1) and is being pulled by the approximately NE moving Iberian plate, which causes the still-active[18,34] N(50°–60°)E extension. The left-lateral motion of the EBSZ[46] is explained by the faster approximately NE-directed Eurasia motion of the offshore Palomares margin (Fig. 2a) with respect to the extending eastern Betic crust (Fig. 1).

Corroborating evidence and APM of the African plate

To investigate the style of the present-day tectonic activity, we inverted the published GPS motions[30,34,47,48] (Fig. 2b and Supplementary Fig. 2) for the underlying strain- and rotation-rate fields, which are independent of the plate-motion frame (Fig. 5, Methods and Supplementary Video 5). These reveal deformation patterns similar to the style of tectonic deformation since 8 Ma, which suggests a time-stationary forcing of crustal deformation: N–S to NE–SW shortening of the Rif, NW–SE shortening of the western Betics and concurrent NNE–NE-directed extension east of the location of active slab tearing[18] (Fig. 5a). The combination of strain- and rotation-rate patterns correctly detects the 'simple shear' nature of the left-lateral EBSZ and WTASZ shear zones and the right-lateral motion of the Yusuf fault, which together help to transfer the absolute N–NNE Africa motion to the NE-directed Eurasian motion as depicted by the flow field (Fig. 5b). The local trans-tensional tectonics and the strike-slip nature of the hazardous earthquakes of the Al Hoceima region[33,49] at the southern extremity of the WTASZ (Fig. 2a) agree with the pattern of the shear-strain rate and is now understood to be caused by slab indentation directly to the west of this region that is driven by mantle-resisted slab dragging.

The predicted crustal flow field (Fig. 5b) in the GMHRF[37] illustrates a close alignment of the absolute Africa and Iberia motion with the WTASZ and EBSZ, respectively. A recent global fixed-hotspot mantle frame[39] (Fig. 3) leads to a similar result. The anomalous approximately SSW-directed GPS motions of the Rif in the Africa-fixed frame[24,43,50] (Fig. 2b) were previously attributed to rollback[22,24,29]. We emphasize, however, that no indication of true rollback, that is, in the mantle frame, can be derived from the GPS motion field (Methods). Instead, the approximate alignment of the GPS vectors in the Rif with the strike of the WTASZ (Fig. 2b) is taken here as a strong indication that the observed indentation is at present driven predominantly by the mantle resistance against approximately NNE slab dragging. This also explains the SW–SSW motion, relative to Africa, of the so-called 'Rif–Betic–west Alboran microplate'[43] as it is coupled to the slab.

From the above analysis we infer that the N 22.5° E±2.5° strike of the WTASZ aligns with the actual direction of the African APM. The alignment of the GPS motions in the mantle frame with the Carboneras fault and EBSZ (Fig. 5b), and our earlier explanation of these fault systems, suggest similarly that their strike of N 51.5° E±2.5° is parallel to the Iberian APM. The rather sharp transition of the APM occurs in crust not underlain by thick lithosphere and is possibly facilitated by past and ongoing slab tearing and delamination[18,20]. Importantly, such inferred APM directions constitute strong constraints on the location of the absolute Euler pole (Methods and Supplementary Fig. 3). Furthermore, these fault-system directions combined with estimates of local relative plate motion even allow us to compute the local APM vector of the African plate (red vector in Fig. 3 and Methods). This APM vector is based on our new interpretation of the origin of both fault systems and is independent of other predictions of APM (Fig. 3). The crustal signature of mantle-resisted slab dragging thus offers a novel way to determine APM directions and better constrain the still rather uncertain (Fig. 3) mantle frame.

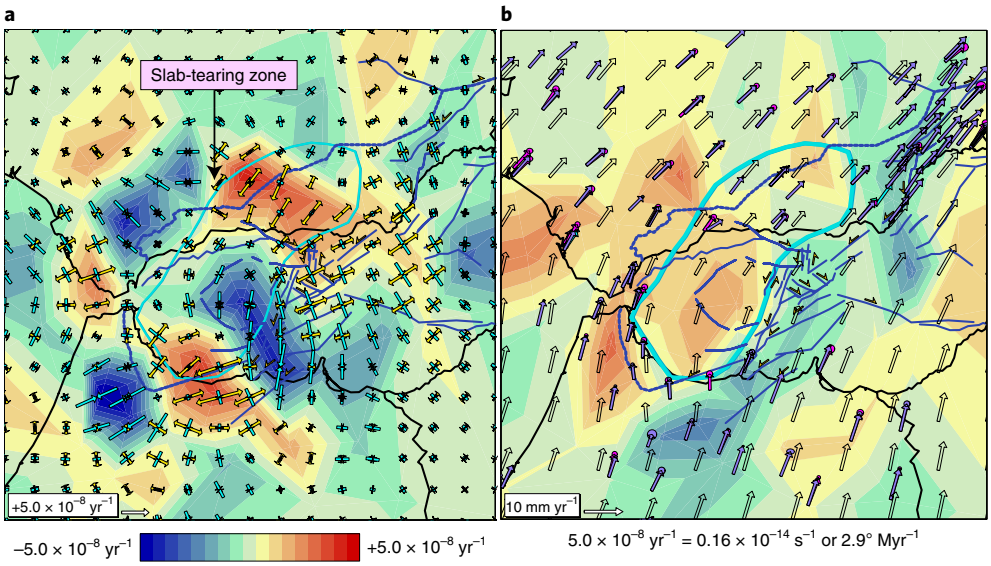

Fig. 5 | GPS-derived strain and rotation rates and crustal motion in the mantle frame. a, Principal axes and amplitudes of strain rate. The light-blue (yellow) vectors denote contraction (extension). The dilation rate is colour contoured; positive (negative) values denote extension (contraction). **b**, Observed (Fig. 2 caption) and predicted crustal motion field in the GMHRF[37]. The rotation rate is colour contoured (legend below **a**; reddish colours show a clockwise rotation).

Our new geodynamic model for the region in a mantle reference frame naturally includes the relative NW–SE convergence between Iberia and Africa and complements this with N–NNE mantle-resisted dragging of a tearing slab. It coherently explains all the first-order tectonic features that were hitherto poorly understood. We identify the WTASZ, Yusuf fault and EBSZ as important fault systems for the transfer from African to Eurasian plate motion, as was suggested previously[22], with the plates still connected through the Rif–Gibraltar–western-Betics corridor (Fig. 1). This implies a nascent, rather than mature, plate boundary, which explains the tectonically diffuse character of the region.

Our analysis corroborates the existence of slab dragging and that its direction can be unrelated to trench orientation or relative plate convergence in the case that the entire subduction system is transported by a common component of the APM of the subducting and overriding plates (Fig. 4a inset), which may be one reason why slab dragging has been largely overlooked since the recognition of plate tectonics. Our definition of slab dragging also comprises the trench-perpendicular contributions of the subducting plate to subduction, slab rollback or slab advance in which the deep upper mantle resistance has been called slab anchoring[1]. The large trench-oblique lateral transport suggested in previous studies[5–8] indicates that the mantle resistance against slab dragging does not necessarily lead to a strong slab anchoring. Slab dragging is only detectable in the mantle frame and its effects on the tectonic evolution of other plate boundary zones remain to be explored.

Methods

Methods, including statements of data availability and any associated accession codes and references, are available at https://doi.org/10.1038/s41561-018-0066-z.

Received: 12 June 2017; Accepted: 15 January 2018;
Published online: 19 February 2018

References

1. Heuret, A. & Lallemand, S. Plate motions, slab dynamics and back-arc deformation. *Phys. Earth Planet. Inter.* **149**, 31–51 (2005).
2. Schellart, W. P., Stegman, D. R. & Freeman, J. Global trench migration velocities and slab migration induced upper mantle volume fluxes: constraints to find an Earth reference frame based on minimizing viscous dissipation. *Earth Sci. Rev.* **88**, 118–144 (2008).
3. Haq, S .S. B. & Davis, D. M. Mechanics of fore-arc slivers: insights from simple analog models. *Tectonics* **29**, 5015 (2010).
4. Chertova, M. V., Spakman, W., van den Berg, A. P. & van Hinsbergen, D. J. J. Absolute plate motions and regional subduction evolution. *Geochem. Geophys. Geosyst.* **15**, 3780–3792 (2014)..
5. Giardini, D. & Woodhouse, J. H. Horizontal shear flow in the mantle beneath the Tonga arc. *Nature* **319**, 551–555 (1986).
6. Spakman, W. & Hall, R. Surface deformation and slab–mantle interaction during Banda arc subduction rollback. *Nat. Geosci.* **3**, 562–566 (2010).
7. Pikser, J. E., Forsyth, D. W. & Hirth, G. Along-strike translation of a fossil slab. *Earth Planet. Sci. Lett.* **331–332**, 315–321 (2012).
8. Le Dain, A. Y., Tapponnier, P. & Molnar, P. Active faulting and tectonics of Burma and surrounding regions. *J. Geophys. Res.* **89**, 453–472 (1984).
9. Platt, J. P. et al. The ultimate arc: differential displacement, oroclinal bending, and vertical axis rotation in the external Betic–Rif arc. *Tectonics* **22**, 1017 (2003).
10. Gutscher, M. A. et al. Evidence for active subduction beneath Gibraltar. *Geology* **30**, 1071–1074 (2002).
11. Spakman, W. & Wortel, M. J. R. in *The TRANSMED Atlas: The Mediterranean Region from Crust to Mantle* (eds Cavazza, W. et al.) 31–52 (Springer, Berlin, 2004).
12. Bezada, M. J. et al. Evidence for slab rollback in western-most Mediterranean from improved upper mantle imaging. *Earth Planet. Sci. Lett.* **368**, 51–60 (2013).
13. Villaseñor, A. et al. Subduction and volcanism in the Iberia–North Africa collision zone from tomographic images of the upper mantle. *Tectonophysics* **663**, 238–249 (2015).
14. Chertova, M. V., Spakman, W., van den Berg, A. P., Geenen, T. & van Hinsbergen, D. J. J. Underpinning tectonic reconstructions of the western Mediterranean region through dynamic slab evolution from 3D numerical modeling. *J. Geophys. Res.* **119**, 5876–5902 (2014).
15. Vergés, J. & Fernandez, M. Tethys–Atlantic interaction along the Iberia–Africa plate boundary: the Betic–Rif orogenic system. *Tectonophysics* **579**, 144–172 (2012).
16. van Hinsbergen, D. J. J., Vissers, R. & Spakman, W. Origin and consequences of western Mediterranean subduction, rollback, and slab segmentation. *Tectonics* **33**, 393–419 (2014).
17. Faccenna, C., Piromallo, C., Crespo-Blanc, A., Jolivet, L. & Rossetti, F. Lateral slab deformation and the origin of the western Mediterranean arcs. *Tectonics* **23**, 1012 (2004).
18. De Lis Mancilla, F. et al. Slab rupture and delamination under the Betics and Rif constrained from receiver functions. *Tectonophysics* **663**, 225–237 (2015).
19. Garcia-Castellanos, D. & Villasenor, A. Messinian salinity crisis regulated by competing tectonics and erosion at the Gibraltar arc. *Nature* **480**, 359–363 (2011).
20. Levander, A. et al. Subduction-driven recycling of continental margin lithosphere. *Nature* **515**, 253–256 (2014).

21. Heit, B. et al. Tearing of the mantle lithosphere along the intermediate-depth seismicity zone beneath the Gibraltar Arc: the onset of lithospheric delamination. *Geophys. Res. Lett.* **44**, 4027–4035 (2017).
22. Gutscher, M. A. et al. The Gibraltar subduction: a decade of new geophysical data. *Tectonophysics* **574–575**, 72–91 (2012).
23. Neres, M., Carafa, M. & Fernandes, R. Lithospheric deformation in the Africa–Iberia plate boundary: improved neotectonic modeling testing a basal-driven Alboran plate. *J. Czech Geol. Soc.* **121**, 6566–6596 (2016).
24. Pérouse, E., Vernant, P., Chéry, J., Reilinger, R. & McClusky, S. Active surface deformation and sub-lithospheric processes in the western Mediterranean constrained by numerical models. *Geology* **38**, 823–826 (2010).
25. Jimenez-Munt, I. & Negredo, A. M. Neotectonic modelling of the western part of the Africa–Eurasia plate boundary: from the Mid-Atlantic ridge to Algeria. *Earth Planet. Sci. Lett.* **205**, 257–271 (2003).
26. Pérouse, E. et al. Bridging onshore and offshore present-day kinematics of central and eastern Mediterranean: implications for crustal dynamics and mantle flow. *Geochem. Geophys. Geosyst.* **13**, 1213–1225 (2012).
27. Flecker, R. et al. Evolution of the Late Miocene Mediterranean–Atlantic gateways and their impact on regional and global environmental change. *Earth Sci. Rev.* **150**, 365–392 (2015).
28. Capella, W. et al. Thick-skinned tectonics closing the Rifian Corridor. *Tectonophysics* **710–711**, 249–265 (2017).
29. Fadil, A. et al. Active tectonics of the western Mediterranean: geodetic evidence for rollback of a delaminated subcontinental lithospheric slab beneath the Rif Mountains, Morocco. *Geology* **34**, 529–532 (2006).
30. Petit, C. et al. Crustal structure and gravity anomalies beneath the Rif, northern Morocco: implications for the current tectonics of the Alboran region. *Geophys J. Int* **202**, 640–652 (2015).
31. Baratin, L.-M. et al. Incipient mantle delamination, active tectonics and crustal thickening in Northern Morocco: insights from gravity data and numerical modeling. *Earth Planet. Sci. Lett.* **454**, 113–120 (2016).
32. Diaz, J., Gil, A., Carbonell, R., Gallart, J. & Harnafi, M. Constraining the crustal root geometry beneath Northern Morocco. *Tectonophysics* **689**, 14–24 (2016).
33. Grevemeyer, I., Gràcia, E., Villaseñor, A., Leuchters, W. & Watts, A. B. Seismicity and active tectonics in the Alboran Sea, Western Mediterranean: constraints from an offshore-onshore seismological network and swath bathymetry data. *J. Geophys. Res. Earth Sci.* **120**, 8248–8365 (2015).
34. Palano, M., González, P. J. & Fernandez, J. The diffuse plate boundary of Nubia and Iberia in the Western Mediterranean: crustal deformation evidence for viscous coupling and fragmented lithosphere. *Earth Planet. Sci. Lett.* **430**, 439–447 (2015).
35. Cunha, T. A. et al. Neotectonics of the SW Iberia margin, Gulf of Cadiz and Alboran Sea: a reassessment including recent structural, seismic and geodetic data. *Geophys J. Int.* **188**, 850–872 (2012).
36. O'Neill, C., Müller, D. & Steinberger, B. On the uncertainties in hot spot reconstructions and the significance of moving hot spot reference frames. *Geochem. Geophys. Geosyst.* **6**, Q04003 (2005).
37. Doubrovine, P. V., Steinberger, B. & Torsvik, T. H. Absolute plate motions in a reference frame defined by moving hot spots in the Pacific, Atlantic, and Indian oceans. *J. Geophys. Res.* **117**, B09101 (2012).
38. Stotz, I. L., Iaffaldano, G. & Davies, D. R. Late Miocene Pacific plate kinematic change explained with coupled global models of mantle and lithosphere dynamics. *Geophys. Res. Lett.* **44**, 7177–7186 (2017).
39. Wang, C., Gordon, R. G. & Zhang, T. Bounds on geologically current rates of motion of groups of hot spots. *Geophys. Res. Lett.* **44**, 6048–6056 (2017).
40. Debayle, E. & Ricard, Y. Seismic observations of large-scale deformation at the bottom of fast-moving plates. *Earth Planet. Sci. Lett.* **376**, 165–177 (2013).
41. Zheng, L., Gordon, R. G. & Kreemer, C. Absolute plate velocities from seismic anisotropy: importance of correlated errors. *J. Geophys. Res. Solid Earth* **119**, 7336–7352 (2014).
42. Becker, T. W., Schaeffer, A. J., Lebedev, S. & Conrad, C. P. Toward a generalized plate motion reference frame. *Geophys. Res. Lett.* **42**, 3188–3196 (2015).
43. Koulali, A. et al. New GPS constraints on active deformation along the Africa–Iberia plate boundary. *Earth Planet. Sci. Lett.* **308**, 211–217 (2011).
44. Platt, J. P., Behr, W. M., Johanesen, K. & Williams, J. R. The Betic–Rif Arc and its orogenic hinterland: a review. *Annu. Rev. Earth Planet. Sci.* **41**, 313–357 (2013).
45. Duggen, S., Hoernle, K., Van der Bogaard, P. & Garbe-Schönenberg, D. Post-collisional transition from subduction-to intraplate-type magmatism: evidence from continental-edge delamination of subcontinental lithosphere. *J. Petrol.* **46**, 1155–1201 (2005).
46. Giaconia, F. et al. Compressional tectonic inversion of the Algero–Balearic basin: Latemost Miocene to present oblique convergence at the Palomares margin (Western Mediterranean). *Tectonics* **34**, 1516–1543 (2015).
47. Echeverria, A., Khazaradze, G., Asensio, E. & Gárate, J. Crustal deformation in eastern Betics from CuaTeNeo GPS network. *Tectonophysics* **608**, 600–612 (2013).
48. de Lis Mancilla, F. et al. Delamination in the Betic Range: deep structure, seismicity, and GPS motion. *Geology* **41**, 307–310 (2013).
49. Lafosse, M. et al. Evidence of quaternary transtensional tectonics in the Nekor basin (NE Morocco). *Basin Res.* **29**, 470–489 (2016).
50. Vernant, P. et al. Geodetic constraints on active tectonics of the Western Mediterranean: implications for the kinematics and dynamics of the Nubia–Eurasia plate boundary zone. *J. Geodyn.* **49**, 123–129 (2010).

Acknowledgements

We thank P. Vernant for helpful comments, A. Villasenor for help with obtaining the regional hypocentral data and M. Bezada for sharing his regional tomography model. W.S. and M.V.C. acknowledge financial and computational support from ISES, the Netherlands research centre for Integrated Solid Earth Science. W.S. also acknowledges support from the Research Council of Norway through its Centres of Excellence funding scheme, project number 223272. D.J.J.v.H. acknowledges ERC Starting Grant 306810 (SINK) and NWO Vidi grant 864.11.004.

Author contributions

W.S. conceived and designed the research and contributed the GPS analysis. M.V.C contributed the numerical modelling with support from A.P.vd.B. D.J.J.v.H. contributed the geological component. W.S. wrote the paper with contributions from D.J.J.v.H.

Competing interests

The authors declare no competing interests.

Additional information

Supplementary information is available for this paper at https://doi.org/10.1038/s41561-018-0066-z.

Reprints and permissions information is available at www.nature.com/reprints.

Correspondence and requests for materials should be addressed to W.S.

Publisher's note: Springer Nature remains neutral with regard to jurisdictional claims in published maps and institutional affiliations.

Methods

APM models. For most of our numerical modelling (B and G models of Fig. 4 and Supplementary Fig. 1, as well as in previous work[4,14]), we adopted the average APM of the African plate of the past ~35 Myr determined from the GMHRF[37]. The GMHRF results from an elaborate iterative scheme that utilizes the latest plate circuits and accounts for hotspot motion due to lateral plume advection in a flowing mantle. The resulting APM frame explains the hotspot tracks well and the model outcomes, such as absolute Euler poles, are given with realistic uncertainty estimates. Several other APM frames exist, but most only apply to the present day or the past few million years[42] (Fig. 3). We used the GMHRF because it is currently the most-elaborated global hotspot frame that links APMs to the deep mantle. Other hotspot frames use subsets of hotspot tracks or are limited to the past few million years (main text).

With regard to our numerical modelling of subduction evolution, we tested several end-member mantle frames (based on Africa-fixed, Iberia-fixed and a model that assumed Africa motion is twice the velocity in the GMHRF) as model boundary conditions to investigate how different plate motions would affect the subduction evolution of the RGB slab[4].

In our illustration of regional GPS motion in the mantle frame (Fig. 5b) we used the Africa APM GMHRF[37] pole for the past 10 Myr (SI Fig. 3). Our work shows independently that this pole is rather well located (Fig. 3 and final section of Methods).

3D numerical modelling of RGB-slab evolution. We largely follow Chertova et al.[4,14] for the 3D slab-evolution modelling of its Tectonic Evolution Scenario 1 for the western Mediterranean region. This tectonic scenario outperformed other published scenarios in predicting the imaged RGB slab structure after 35 Myr of subduction evolution. The initial model set-up, a Cartesian box of 1,000 km × 1,800 km × 1,300 km in N–S, E–W and depth extent, respectively, describes the ocean–continent palaeogeography and initial subduction at ~35 Ma (ref. [16]). The latter concerns a small slab restricted to the Baleares margin that starts to rollback initially to the south, then turns to the west and, in the final stages, rolls back to the NW (Supplementary Videos 2–4). Numerical modelling of this evolution is based on the extended Boussinesq approximation, which includes upper-mantle phase changes and frictional heating. Although we solve the same pertinent equations as in Chertova et al.[4,14], we show these equations for completeness and for the definition of the specific use and setting of the model parameters that appear in the equations (Supplementary Table 1). We use the finite-element modelling package SEPRAN[51] to solve the following dimensionless equations (summation over repeated indices is implied).

The mass conservation of an incompressible viscous fluid:

$$\partial_j v_j = 0 \tag{1}$$

Stokes equation:

$$-\partial_i P + \partial_j \tau_{ij} = \left(\mathrm{Ra} T - \sum_k \mathrm{Rb}_k \Gamma_k \right) g_i \tag{2}$$

and the heat-conservation equation:

$$\frac{\partial T}{\partial t} + v_j \partial_j T - \partial_j \partial_j T - \mathrm{Di}(T + T_0) g_i v_i - \sum_k \gamma_k \frac{\mathrm{Rb}_k}{\mathrm{Ra}} \mathrm{Di}(T + T_0) \frac{\mathrm{d}\Gamma_k}{\mathrm{d}t} = \frac{\mathrm{Di}}{\mathrm{Ra}} \Phi \tag{3}$$

A composite viscoplastic rheology is used that comprises dislocation and diffusion creep and a stress limiter. The effective viscosity η_{eff} is determined as:

$$\frac{1}{\eta_{\mathrm{eff}}} = \frac{1}{\eta_{\mathrm{diff}}} + \frac{1}{\eta_{\mathrm{disl}}} + \frac{1}{\eta_y} \tag{4a}$$

where

$$\eta_{\mathrm{diff}} = \mu\, A_{\mathrm{diff}}^{-1} (b/d)^{-m} \exp\left[(E_{\mathrm{diff}} + P V_{\mathrm{diff}}) / RT \right] \tag{4b}$$

$$\eta_{disl} = \mu\, A_{\mathrm{disl}}^{-\frac{1}{n}} \dot{\varepsilon}^{\frac{1-n}{n}} \exp\left[(E_{\mathrm{disl}} + P V_{\mathrm{disl}}) / nRT \right] \tag{4c}$$

$$\eta_y = \frac{\tau_y}{2\dot{\varepsilon}} \tag{4d}$$

and

$$\tau_y = \min(\tau_0 + \gamma P, \tau_{\max}) \tag{4e}$$

In these equations v is the flow velocity; τ is the mechanical stress; Ra is the thermal Rayleigh number; Rb is the compositional Rayleigh number, Γ is the phase function; g is the gravitational acceleration; Di is the dissipation number; Φ is the fractional dissipation; η is the power law exponent; $\dot{\varepsilon}$ is the second invariant of the strain-rate tensor; $A_{\mathrm{diff,disl}}$ are diffusion and dislocation creep viscosity prefactors; μ is the shear modulus; γ is the yield stress gradient; b is the Burgers vector; d is the grain size; m is the grain-size exponent; $V_{\mathrm{diff,disl}}$ and $E_{\mathrm{diff,disl}}$ are the activation volume and activation energy for diffusion and dislocation creep, respectively; P is the lithostatic pressure; T is the temperature; τ_0 is the yield stress value at the top surface and $\tau_{\max}$ is the maximum yield stress value. The first component of τ_y defines the depth-dependent strength of the material. If the stress exceeds this value the material gradually becomes weaker. The strength of the material increases with depth until it reaches $\tau_{\max}$.

Previous models[4,14] used a constant APM velocity for the African and Iberian plate along the southern and northern boundaries of the model. Here we implemented a linear increase from 6.2 mm yr^{-1} in the west to 8.6 mm yr^{-1} in the east imposed at an angle N9° E on the top 150 km of the southern model edge, that is, the lower side in Supplementary Video 2, and is an average of 35 Myr of Africa motion derived from the GMHRF[37] for that boundary. For Iberia we used 4.6 mm yr^{-1} uniformly at an azimuth of N58° E defined at the top 150 km of the northern edge of the model. Below this depth the side boundaries are open for lateral in- or outflow[14]. Instead of a linear mantle geotherm, we now use an adiabatic geotherm with a potential temperature of 1,573 K at a depth of 140 km.

The top surface has a free-slip (impermeable) boundary condition. To allow for slab decoupling from the surface, we followed our previous work by implementing a relatively weak crustal layer of 5.0×10^{19} Pa s and a thickness of 30 km. The numerical models focus on the dynamic evolution of the mechanically strong lithospheric mantle. Our predictions for the first-order tectonic features are primarily governed by the regional dynamic interaction between the rheologically strong lithospheric plates and the slab. Its high age of 100–140 Myr means the slab acts as a stress guide that transmits stresses from the mantle to the overlying crust.

We present results from two slab-evolution models: the 'green' model (G model) of Fig. 4 and the 'blue' model (B model) of Supplementary Fig. 1. Previous models[4,14] showed a relatively large indentation of the Moroccan margin due to mantle-resisted slab dragging. Here we recomputed slab models with slightly different rheological settings (Supplementary Table 1) that showed small, ~10–15 km for the G model (Fig. 4), and large, ~30–35 km for the B model (Supplementary Fig. 1), indentations. The difference between the G and B models results only from a small change in the lower mantle viscosity from 1.0×10^{22} Pa s to 2.0×10^{22} Pa s, respectively, and from a change in the activation energy for diffusion creep from 240 kJ mol^{-1} to 250 kJ mol^{-1}, respectively. The main differences between the two models concern, for the G-model, more slab tearing under the Betics, a smaller indentation of the African margin and some sinking of the G slab in the lower mantle, which partly drives slab tearing under the central–eastern Betics. These differences are due to only small changes in the rheological parameters, which shows how sensitive slab evolution is to nonlinear rheology.

Supplementary Video 2 shows the entire evolution of the G model from a depth of 200 km downward. The slab contours of Fig. 4 are determined from this temporal evolution. Supplementary Videos 3 and 4 show the G model and the B model, respectively, from a viewpoint in the northeast, which clearly illustrates the N–NNE slab dragging of the RGB slab by the African plate.

GPS motion inversion for strain- and rotation-rate fields. The GPS motion inversion was performed with the method developed by Spakman and Nyst[52]. We used published GPS motion vectors[34,43,47,48]. The inversion method inverts the relative motion between all the possible pairs of GPS stations and determines the horizontal velocity-gradient field and the relative Euler rotations between the contributing GPS networks. These relative network rotations are then applied to the data to rotate all the data in a common frame and next an inversion is performed that leads to strain and rotation rates that are no longer significantly affected by relative network rotations. We supplemented this data set with 12 synthetic motion vectors on the African plate, 10 in the Atlantic and 2 in Algeria (Supplementary Fig. 2), which were assigned a 0 ± 0.2 mm yr^{-1} motion in the African frame. In the Atlantic, these synthetic data force the velocity gradient to zero, whereas in Algeria they help to stabilize the solution near the boundary. In the Atlantic, the synthetic data determine only the transition in deformation from the land to ocean and do not affect the deformation patterns discussed in the main text. Supplementary Fig. 2 also shows the model triangulation of the larger region for which we performed the GPS inversion using triangles on which bilinear basis functions are defined for the model parameters (the four independent components of the strain- and rotation-rate tensors in a spherical geometry), which allows for a quadratic velocity change within each model triangle.

The inversion results shown in Fig. 5 are a zoom-in on the study region. The inversion of the GPS vectors requires some regularization to stabilize the solution near the network perimeter where data density is low. The solution on the perimeter can be regularized separately and has been used to force the velocity gradient to zero. In addition, we experimented with imposed damping on the amplitudes of the components of the velocity-gradient tensor field. Supplementary Video 5 shows how additional uniform amplitude damping affects the solution and the prediction of the crustal flow field as well as the spatial resolution and model covariance. For the definition of spatial resolution and model covariance we refer

to the original paper[52]. The solution discussed in Fig. 5 of belongs to the start of Supplementary Video 5 (no amplitude damping except for the model perimeter) and is very well resolved with relative amplitude errors less than 2%.

GPS motions, slab rollback and the plate boundary. The method to define slab rollback, or advance, principally requires a mantle frame of reference, in practise a frame attached to the lower mantle[37], such that the trench-normal motion of the slab relative to the mantle can be determined[1]. Previously, however, anomalous GPS motions in the Moroccan Rif, as displayed in the African-fixed reference frame (Fig. 2b), have been attributed to W–WSW[22] or SSW[24] directed RGB-slab rollback. Fig. 5b shows the GPS motion field in the mantle frame of Doubrovine et al.[37] using the Africa pole for the past 10 Myr. This Africa pole predicts surface motions that are relatively close to what we independently infer here (main text and see below). This representation of the crustal flow field gives no indication of slab rollback to the W–WSW of SSW. Instead it is evident in this mantle frame that the crust that overlies the slab moves to the N–NNE in concert with the African and Iberian lithosphere, and thus the entire slab, attached to both plates, is following this motion, which we call slab dragging. Anomalous motion that does not follow this general N–NNE slab transport is still seen in the Moroccan Rif (Fig. 5b), which we explain in the main text as the slab-indentation effect due to the mantle resistance against slab dragging.

Accepting the lateral shape of the slab as imaged by independent seismic tomography experiments[10–14] (Fig. 1 and Supplementary Video 1), buoyancy-driven rollback, if any, can only be directed to the W–NW, that is, perpendicular to the slab shape in the mantle frame (for example, Supplementary Fig. 1). Supplementary Fig. 2 shows the GPS motion vectors with respect to mainland Iberia using the Iberia-–Nubia pole of Palano et al.[34]. Only in the Iberia-fixed frame the seemingly westward motion of predominantly the western–central Betics and Gibraltar Strait may be suggestive of western-slab rollback. This motion pattern of the Betics in the Iberian frame is, however, entirely attributable to the use of the Iberian-fixed reference frame for display, which cancels the NE absolute motion of the Iberian mainland[37] (Fig. 5b and Supplementary Fig. 2). This NE Iberian motion is apparently not followed by the western–central Betics and only partly by the eastern Betics. The western Betics are still coupled to the slab[18,21] (Fig. 1) and follow the slab motion (Figs. 2b and 5b). Hence, there is no conclusive evidence in the GPS motion field for identifying slab rollback. Slab motion in a mantle frame other than that resulting from buoyancy-driven trench-normal slab rollback would require another forcing, as put forward in this paper.

The display of motions in the Iberian reference frame (Supplementary Fig. 2) does, however, support the suggestion[22] that the plate boundary deformation occurring between the Gulf of Cadiz and the eastern-plate fault systems, WTASZ and EBSZ, defines a motion-transfer zone that involves the crust of the Betics, rather than a plate boundary elsewhere[23,50].

Determination of the local APM vectors. We compute the APM vectors at location 3.5° W, 36° N, simulating the intersection point of the WTASZ and the Carboneras fault (Fig. 2), using the inferred directions $\mathbf{n}_A$ for the African APM of N 22.5° E ± 2.5° and $\mathbf{n}_E$ for the Eurasia APM of N 51.5° E ± 2.5°, where $\mathbf{n}_A$ and $\mathbf{n}_E$ are unit vectors. Using the observed relative motion Δv_{EA} of the Eurasian plate relative to the Africa plate, we can solve the equation $s_E n_E - s_A n_A = \Delta v_{EA}$ for the amplitudes s_E and s_A of the Eurasian and African APMs. Relative plate motions are determined in various ways, for example, from an analysis of geologically recent seafloor-spreading rates and fault azimuths (MORVEL[53]) or from geodetic observations of the present day (for example, SEGAL2013[54,55]). These estimates do not need to coincide if the current relative plate motions have changed with respect to the average over the past few million years[53], and using different geodetic data sets may lead to slightly different relative plate motion estimates. The relative motion determined from MORVEL is 3.3 mm yr^{-1} to the east and 3.9 mm yr^{-1} to the south. In model SEGAL2013, the relative motion is 4.8 mm yr^{-1} to the east and 2.9 mm yr^{-1} to the south. Lastly, the relative motion computed from the poles of Palano et al.[34] is 4.5 mm yr^{-1} to the east and 2.3 mm yr^{-1} to the south. We computed the magnitudes s_E and s_A of the absolute Africa and Eurasia motion across all combinations of relative motion vectors and azimuths. This leads to the absolute motion of Africa at the location 3.5° W, 36° N to 10.6 ± 2.5 mm yr^{-1} in the direction N 22.5° E ± 2.5°, and for the Eurasian plate to 10.8 ± 2.9 mm yr^{-1} in the direction N 51.5° E ± 2.5°. The given uncertainties in the APM estimates encompass all variations in the relative plate motion and fault-strike observations. These APM estimates are derived from kinematic geological data and geodetic data, both essentially relative kinematic observations by nature.

Figure 3 shows our APM motion vector for the African plate (red vector). It is significantly different from those of the GMHRF and other predictions, but follows the trend of global hotspot mantle frames. The GMHRF Euler pole for the absolute Africa motion of the past 10 Myr is rather uncertain (Supplementary Fig. 3), as is reflected by its local prediction (Fig. 3). The single prediction of APM that we make here constitutes a strong constraint for determining the Euler pole location because the Euler pole is located on the great circle perpendicular to that estimated direction (Supplementary Fig. 3). Hence, only two of such direction estimates in spatially separated points would suffice to improve considerably the GMHRF Euler pole position by refining the Euler pole's confidence region (Supplementary Fig. 3).

Code availability. The SEPRAN finite element code used to generate the subduction models is a commercial code that can be assessed through the code developers[51].

Data availability. The tomographic model UU-P07 is available at http://www.atlas-of-the-underworld.org. GPS data sets are available through the respective publications.

References

51. Segal, G. & Praagman, N. P. *The SEPRAN FEM package* Technical report (Ingenieursbureau Sepra, Leidschendam, 2005).
52. Spakman, W. & Nyst, M. Inversion of relative motion data for estimates of the velocity gradient field and fault slip. *Earth Planet. Sci. Lett.* **203**, 577–591 (2002).
53. DeMets, C., Gordon, R. G. & Argus, D. F. Geologically current plate motions. *Geophys J. Int.* **181**, 1–80 (2010).
54. Fernandes, R. M. S. The relative motion between Africa and Eurasia as derived from ITRF2000 and GPS data. *Geophys. Res. Lett.* **30**, 1828 (2003).
55. Fernandes, R., Miranda, J M., Delvaux, D., Stamps, D S. & Saria, E. Re-evaluation of the kinematics of Victoria Block using continuous GNSS data. *Geophys. Res. Lett.* **193**, 1–10 (2013).